# The Catalytic Subunit of *Escherichia coli* Nitrate Reductase A Contains a Novel [4Fe-4S] Cluster with a High-Spin Ground State[†,‡]

Richard A. Rothery,[§] Michela G. Bertero,[||] Richard Cammack,[⊥] Monica Palak,[§] Francis Blasco,[#] Natalie C. J. Strynadka,[||] and Joel H. Weiner*[,§]

*CIHR Membrane Protein Research Group, Department of Biochemistry, University of Alberta, 474 Medical Sciences Building, Edmonton, Alberta T6G 2H7, Canada, Department of Biochemistry, University of British Columbia, 2146 Health Sciences Mall, Vancouver, British Columbia V6T 1Z3, Canada, Department of Life Sciences, King's College London, Franklin-Wilkins Building, 150 Stamford Street, London SE1 9NN, U.K., and Laboratoire de Chimie Bactérienne, CNRS, 31 chemin Joseph Aiguier, 13402 Marseille Cedex 9, France*

*Received January 8, 2004; Revised Manuscript Received March 3, 2004*

ABSTRACT: We have used EPR spectroscopy, redox potentiometry, and protein crystallography to characterize the [4Fe-4S] cluster (FS0) of the *Escherichia coli* nitrate reductase A (NarGHI) catalytic subunit (NarG). FS0 is clearly visible in the crystal structure of NarGHI [Bertero, M. G., et al. (2003) *Nat. Struct. Biol. 10*, 681−687] but has novel coordination comprising one His residue and three Cys residues. At low temperatures (<15 K), reduced NarGHI exhibits a previously unobserved EPR signal comprising peaks at $g = 5.023$ and $g = 5.556$. We have assigned these features to a $[4Fe\text{-}4S]^{+}$ cluster with an $S = {}^{3}/_{2}$ ground state, with the $g = 5.023$ and $g = 5.556$ peaks corresponding to subpopulations exhibiting $\Delta S = {}^{1}/_{2}$ and $\Delta S = {}^{3}/_{2}$ transitions, respectively. Both peaks exhibit midpoint potentials of approximately −55 mV at pH 8.0 and are eliminated in the EPR spectrum of apomolybdo-NarGHI. The structure of apomolybdo-NarGHI reveals that FS0 is still present but that there is significant conformational disorder in a segment of residues that includes one of the Cys ligands. On the basis of these observations, we have assigned the high-spin EPR features of reduced NarGHI to FS0.

*Escherichia coli*, when grown anaerobically with nitrate as respiratory oxidant, develops a respiratory chain terminated by a membrane-bound quinol:nitrate oxidoreductase (NarGHI)[1] (*1*, *2*). This enzyme can be overexpressed to high levels in the cytoplasmic membrane (*3*) and has been subjected to intense biochemical, biophysical, and structural scrutiny. It comprises a molybdenum cofactor-containing [molybdo-bis(molybdopterin guanine dinucleotide), Mo-bisMGD] catalytic subunit (NarG; 139 kDa), an [Fe-S] cluster-containing electron transfer subunit (NarH; 58 kDa), and a heme-containing membrane-anchor subunit (NarI; 26 kDa) (*2*, *4*−*7*). The catalytic and electron transfer subunits comprise a cytoplasmically localized membrane-extrinsic catalytic dimer (NarGH) anchored to the membrane by NarI. The structure of the enzyme has recently been solved to 1.9 Å resolution (*2*).

Electron transfer through NarGHI occurs between a quinol binding site (Q-site) located toward the periplasmic side of NarI (*3*, *8*−*10*) and the Mo-bisMGD cofactor in NarG (*4*, *7*). Electrons derived from the oxidation of quinol (menaquinol or ubiquinol) are transferred through two hemes in NarI (hemes $b_D$ and $b_P$), four [Fe-S] clusters in NarH (one [3Fe-4S] cluster, FS4, and three [4Fe-4S] clusters, FS3−FS1), and one [4Fe-4S] cluster in NarG (FS0) to the Mo-bisMGD cofactor where nitrate is reduced to nitrite. These centers are arranged in an arc joining the Q-site to the nitrate binding site in the following order: quinol → $b_D$ → $b_P$ → FS4 → FS3 → FS2 → FS1 → FS0 → Mo-bisMGD → $NO_3^-$ (*2*). This arrangement of prosthetic groups is similar to that observed in the structure of *E. coli* formate dehydrogenase N (*11*), except that the direction of electron flow is reversed. With the exception of FS0, clear EPR evidence exists for all of the prosthetic groups of NarGHI. Prior to the availability of its structure, a comprehensive picture of the coordination of the hemes and NarH [Fe-S] clusters (FS1−FS4) was obtained using a combination of EPR spectroscopy, redox potentiometry, and site-directed mutagenesis (*3*, *5*, *6*, *12*, *13*). Although complicated by intercenter spin−spin interactions, FS1, FS2, FS3, and FS4 exhibit relatively

[†] This work was funded by the Canadian Institutes of Health Research, the Canada Foundation for Innovation, the National Institutes of Health, the Human Frontier Science Program Organization, the Howard Hughes Medical Institute, and the Alberta Heritage Foundation for Medical Research. R.C. was supported by a Visiting Scientist award from the Alberta Heritage Foundation for Medical Research. J.H.W. is a Canada Research Chair in Membrane Biochemistry.

[‡] The atomic coordinates and structure factors of the structure determined in this work have been deposited with the Brookhaven Protein Data Bank as entry 1SIW.

* To whom correspondence should be addressed. Tel: (780) 492-2761. Fax: (780) 492-0886.

[§] University of Alberta.

[||] University of British Columbia.

[⊥] King's College London.

[#] Laboratoire de Chimie Bactérienne, CNRS.

[1] Abbreviations: DmsABC, *Escherichia coli* $Me_2SO$ reductase; FrdABCD, *E. coli* fumarate reductase; HALS, highly anisotropic low spin; IPTG, isopropyl 1-thio-β-D-galactopyranoside; Mo-bisMGD, molybdo-bis(molybdopterin guanine dinucleotide); NarGHI, nitrate reductase.

10.1021/bi049938l CCC: $27.50 
Published on Web 04/17/2004

```
Type 1
napa_parpn 42TWSKAPCRF.CGTGCGVMVGVKEG.......RVVATHGDLLAEVNRGLNCVKGYFLSKIM
napa_rhosh 42RWSKAPCRF.CGTGCGVMVGTRDG.......QVVATHGDTQAEVNRGLNCVKGYFLSKIM
napa_ecoli 40KWDKAPCRF.CGTGCGVLVGTQQG.......RVVACQGDPDAPVNRGLNCIKGYFLPKIM
napa_desde 39KWVKGVCRY.CGTGCGVLVGVKDG.......KAVAIQGDP.NNHNAGLLCLKGSLLIPVL
fdng_ecoli 44KEIRNTCTY.CSVGCGLLMYSLGDGAKNAREAIYHIEGDPDHPVSRGALCPKGAGLLDYV
fdog_ecoli 44RETRNTCTY.CSVGCGLLMYSLGDGAKNAKASIFHIEGDPDHPVNRGALCPKGAGLVDFI
fdha_wolsu 55KKVKTICTY.CSVGCGIIAEVVDG.......VWVRQEVAQDHPISQGGHCCKGADMIDKA
fdhf_ecoli  2KKVVTVCPY.CASGCKINLVVDNG.......KIVRAEAAQ.GKTNQGTLCLKGYYGWDFI
Consensus    ------C--.C--GC------------------------------G--C-KG-------

Type 2
narg_ecoli 43KIVRSTHGVNCTGSCSWKIYVKNGLVTWETQQTDYPRTRPDLPNHEPRGCPRGASYSWYL
narz_ecoli 43KIVRSTHGVNCTGSCSWKIYVKNGLVTWEIQQTDYPRTRPDLPNHEPRGCPRGASYSWYL
narg_bacsu 48KVVRSTHGVNCTGSCSWNIYVKNGIVTWEGQNLNYPSTGPDMPDFEPRGCPRGASFSWYI
dmsa_ecoli 57KVIWSACTVNCGSRCPLRMHVVDGEIKY..VETDNTGDDNYDGLHQVRACLRGRSMRRRV
dmsa_haein 48RIVWSACTVNCGSRCPLRMHVKDNRITY..VETDNTGTETYNLDHQVRACLRGRSMRRRV
Consensus    ----S-C-VNC---C-----V------------------------R-C-RG-------
```

FIGURE 1: Sequence alignment of the N-terminal Cys group from a range of molybdoenzyme catalytic subunits. Underlined sequence titles have known structure. napa_parpn: periplasmic nitrate reductase from *P. pantotrophus* (*T. pantotropha*). napa_rhosh: periplasmic nitrate reductase from *R. sphaeroides*. napa_ecoli: periplasmic nitrate reductase from *E. coli*. napa_desdn (*17*): periplasmic nitrate reductase from *D. desulfuricans*. fdng_ecoli: formate dehydrogenase from *E. coli* (*11*). fdog_ecoli: alternate formate dehydrogenase from *E. coli*. fdha_wolsu: formate dehydrogenase from *Wolinella succinogenes*. fdhf_ecoli: formate hydrogen lyase from *E. coli* (*18*). narg_ecoli: nitrate reductase A from *E. coli*. narz_ecoli: nitrate reductase Z from *E. coli* (*2*). narg_bacsu: nitrate reductase from *Bacillus subtilis*. dmsa_ecoli: DMSO reductase from *E. coli*. dmsa_haein: DMSO reductase from *Haemophilus infuenzae*. Sequence alignments were carried out using the ClustalW algorithm (*53*).

conventional EPR spectra with features around $g = 2$, whereas the hemes have spectra typical of highly anisotropic low-spin (HALS) *b*-type cytochromes with $g_z > 3.3$.

No experimental evidence existed for FS0 prior to its observation in the crystal structure of NarGHI (*4*, *6*, *7*, *14*, *15*). However, [4Fe-4S] and [3Fe-4S] clusters have been observed in the catalytic subunits of other members of the Mo-bisMGD-containing bacterial molybdoenzyme family, initially by EPR spectroscopy in the periplasmic nitrate reductase from *Paracoccus pantotrophus* (*Thiosphaera pantotropha*) (NapA) (*16*) and subsequently by X-ray crystallography in NapA from *Desulfovibrio desulfuricans* (*17*) and in the Mo-bisMGD-containing subunit (FdhF) of *E. coli* formate−hydrogen lyase (*18*). The EPR spectrum of FS0 from *P. pantotrophus* NapA is similar to that of a typical $[4Fe\text{-}4S]^{+}$ cluster with *g* values around 2.00 ($g_z = 2.03$, $g_y = 1.94$, $g_x = 1.89$) and a midpoint potential of −160 mV (*16*). The $[4Fe\text{-}4S]^{+}$ cluster of FdhF also appears to exhibit a conventional EPR spectrum with $g_z = 2.04$, $g_y = 1.96$, and $g_x = 1.84$ (*19*). In the case of wild-type *E. coli* $Me_2SO$ reductase (DmsABC), no EPR evidence exists for the presence of FS0 in its catalytic subunit (DmsA) (*20*, *21*). However, a [3Fe-4S] cluster is assembled into mutants of one of the four conserved Cys residues (DmsA-C67) located toward its N-terminus (*22*). In the case of NarGHI, it has been observed that one of the potentiometrically identified $[4Fe\text{-}4S]^{+}$ clusters exists in two subpopulations with subtly different EPR properties (*15*). It has been speculated that one of these arises from the FS0 cluster (*23*).

All of the [4Fe-4S] clusters observed in the molybdoenzyme catalytic subunits are coordinated by a conserved sequence which includes four Cys residues or one His residue and three Cys residues (a Cys group) located toward their N-termini. Sequence alignments allow assignment of Cys group sequences to two families (Figure 1) (*22*): Type 1, which have two residues between the first two Cys residues, and Type 2, which have three residues between the first two Cys residues (a His and a Cys in the case of NarG). FS0 clusters for which EPR evidence currently exists are coordinated by Type 1 sequences. [4Fe-4S] clusters coordinated by sequences with three residues between the first two cluster-coordinating residues (Type II) are comparatively rare. Examples include [4Fe-4S] clusters found in the bacterial hydrogenases, such as the [Ni-Fe] hydrogenase from *Desulfovibrio gigas* (*24*) and the Fe-only hydrogenase from *Clostridium pasteurianum* (*25*).

In this paper, we have characterized the FS0 [4Fe-4S] cluster of NarG by using a combination of EPR spectroscopy, redox potentiometry, and protein crystallography. We demonstrate that reduced FS0 exhibits a novel EPR spectrum arising from a species with an $S = {}^3/_2$ ground state and that the observation of this species is dependent on the presence of Mo-bisMGD in NarG. Potentiometric studies indicate that the $E_m$ of FS0 renders it competent to undergo redox cycling during enzyme turnover.

## MATERIALS AND METHODS

*Bacterial Strains and Plasmids. E. coli* LCB79 [*ara*D139 Δ(*lac*IPOZYA-*arg*F) *rps*L, *thi* $\phi$79(*nar-lac*)] (*26*) was used as the host for all of the experiments described herein. NarGHI was expressed from plasmid pVA700 (*6*). *E. coli* TP1000 [$F^-$ Δ*lacU169 araD139 rpsL150 relA1 ptsF rbsR flbB* Δ(*mobAB*) $Strep^R$] (*27*) is a *mobAB* deletion mutant that does not assemble the Mo-bisMGD cofactor into NarG during NarGHI maturation (*7*).

*Growth of Cells. E. coli* LCB79/pVA700 was grown overnight in 5 L batches with a 1% inoculum in a B. Braun Biostat B fermenter at 30 °C in the presence of 100 $\mu$g $mL^{-1}$

ampicillin and 100 $\mu$g mL$^{-1}$ streptomycin. The growth medium contained 12 g L$^{-1}$ tryptone, 24 g L$^{-1}$ yeast extract, 5 g L$^{-1}$ NaCl, 4 mL L$^{-1}$ glycerol, and 0.1 mM ammonium molybdate. NarGHI overexpression was induced with 1 mM IPTG at $OD_{600} = 2.0$, after which the cultures were grown for 10−11 h. For overexpression of apomolybdo-NarGHI, cultures were supplemented with 15 mM sodium tungstate. TP1000/pVA700 was grown in 2 L batch cultures in 6 L conical flasks with a 10% inoculum. In this case, the growth medium was Terrific Broth (*28*), and NarGHI overexpression was induced by addition of 0.2 mM IPTG at inoculation. Cells were harvested by centrifugation, washed in a buffer containing 100 mM MOPS and 5 mM EDTA, frozen in liquid nitrogen, and stored at −70 °C prior to use.

*Isolation of Membrane Fractions and Purified Preparations*. Crude membrane vesicles were prepared from *E. coli* cells by French pressure cell lysis and differential centrifugation as previously described (*29*). Enriched inner membrane vesicles were prepared from these crude membranes by sucrose step centrifugation as previously described (*3*). All membrane preparation steps were carried out in a buffer containing 100 mM MOPS and 5 mM EDTA (pH 7.0). Excess sucrose was removed by resuspension and recentrifugation in this buffer. For EPR experiments on enriched membranes, these were resuspended and recentrifuged in a buffer containing 100 mM Tricine and 5 mM EDTA (pH 8.0). For EPR experiments on purified NarGHI (native and apomolybdo), enzyme was prepared by anion-exchange chromatography on a DEAE-FF column (Pharmacia) as described by Bertero et al. (*2*), except that the buffers used contained 50 mM Tricine, 5 mM EDTA, 10% (v/v) glycerol, and 0.05% Thesit (Fluka). Membrane and purified samples were flash frozen in liquid nitrogen and subsequently stored at −70 °C prior to use.

*Redox Potentiometry and EPR Spectroscopy*. Redox titrations were carried out under argon at 25 °C as previously described (*3*, *8*) in 100 mM Tricine and 5 mM EDTA (pH 8.0). The protein concentration used was approximately 30 mg mL$^{-1}$. The following redox mediators were used at a concentration of 50 $\mu$M: quinhydrone, 2,6-dichloroindophenol, 1,2-naphthoquinone, toluylene blue, phenazine methosulfate, thionine, duroquinone, methylene blue, resorufin, indigotrisulfonate, indigodisulfonate, anthraquinone-2-sulfonic acid, phenosafranine, benzyl viologen, and methyl viologen. Non-potentiometrically poised reduced samples were prepared by anaerobic incubation of purified NarGHI with 5 mM dithionite for 10 min at 23 °C. All samples were prepared in 3 mm internal diameter quartz EPR tubes, rapidly frozen in liquid nitrogen-chilled ethanol, and stored under liquid nitrogen until use. EPR spectra were recorded using a Bruker Elexys spectrometer equipped with an Bruker SHQE cavity and an Oxford Instruments ESR-900 flowing helium cryostat. Spectra were recorded under a range of conditions of temperature and microwave power as described in the individual figure legends. Estimates of $E_m$ were obtained from $n = 1$ fits of potentiometric spectral data to the Nernst equation. For studies of the Mo(V) signal of NarGHI, a Bruker ESP300E spectrometer equipped with a $TE_{102}$ microwave cavity and a Bruker liquid nitrogen evaporating cryostat was used (a Bruker ER4111 VT variable temperature unit). In this case, spectra were recorded at 150 K.

Table 1: Data Collection and Refinement Statistics for Apomolybdo-NarGHI

| | |
|---|---|
| data collection | |
| space group | $C222_1$ |
| unit cell (Å), *a*, *b*, *c* | 154.0, 241.3, 140.4 |
| wavelength (Å) | 1.0781 |
| resolution range (Å) | 50−2.2 |
| no. of observations | 579171 |
| unique observations | 128989 |
| completeness (%)[a] | 97.9 (85.2) |
| $R_{sym}$[a,b] | 0.084 (0.351) |
| $\langle I/\sigma \rangle$[a] | 14.3 (2.8) |
| refinement | |
| $R_{cryst}$[c] | 0.203 |
| $R_{free}$[c] | 0.244 |
| average *B*-factor (Å$^2$)[d] | 34.9 |
| rmsd bond lengths (Å) | 0.006 |
| rmsd bond angles (deg) | 1.3 |
| PDB entry | 1SIW |

[a] Values in parentheses represent the highest resolution shell (2.28−2.20 Å). [b] $R_{sym} = \sum_i |I_i - \langle I \rangle| / \sum I_i$, where $i$ is the $i$th measurement and $\langle I \rangle$ is the weighted mean of $I$. [c] $R_{cryst} = \sum ||F_o| - |F_c|| / \sum |F_o|$, where $R_{free}$ is the validation $R$ factor using the test set of 8% of the total data omitted from refinement. [d] The *B*-factor (temperature factor) represents all atoms.

*Protein Assays*. Protein concentrations were assayed by the Lowry method (*30*), modified by the inclusion of 1% (w/v) sodium dodecyl sulfate in the incubation mixture to solubilize membrane proteins (*31*).

*Crystallization, Data Collection, and Structure Determination of Apomolybdo-NarGHI*. Highly ordered crystals of apomolybdo-NarGHI were obtained as described for the native enzyme (*2*). A single data set was collected at 100 K at the Advanced Light Source (beamline 8.2.1). The crystals were isomorphous with the native ($C222_1$, $a = 154.00$ Å, $b = 241.28$ Å, $c = 140.39$ Å). Data were integrated and scaled with the HKL suite of programs (*32*). The structure was determined using difference Fourier techniques and was refined following rigid body refinement of the native 1.9 Å resolution model (*2*) with the CNS program (*33*). Further cycles of manual rebuilding with Xfit (*34*) and refinement with CNS resulted in a final model of apomolybdo-NarGHI with $R_{cryst}$ and $R_{free}$ values of 0.203 and 0.244, respectively. A summary of data collection and refinement statistics is shown in Table 1.

Coordinates and structure factors of the apomolybdo-NarGHI structure have been deposited in the Protein Data Bank with the accession code 1SIW.

## RESULTS

*Previously Unobserved Low-Field Features of the NarGHI EPR Spectrum*. The EPR properties of the three [4Fe-4S] clusters (FS1−FS3) and one [3Fe-4S] cluster (FS4) of NarH have been thoroughly characterized (*6*, *7*, *15*). Although complicated by spin−spin interactions, these clusters all have EPR spectral features that are between approximately $g = 1.8$ and $g = 2.2$. We therefore decided to scrutinize alternative regions of the EPR spectrum in our search for the EPR spectrum of the NarG FS0 [4Fe-4S] cluster. On the basis of its novel coordination (one His residue and three Cys residues), we speculated that it may have a high spin ($S = {}^3/_2$ ground state) (*35*, *36*). We therefore scrutinized the low-field region of the EPR spectrum of reduced NarGHI.

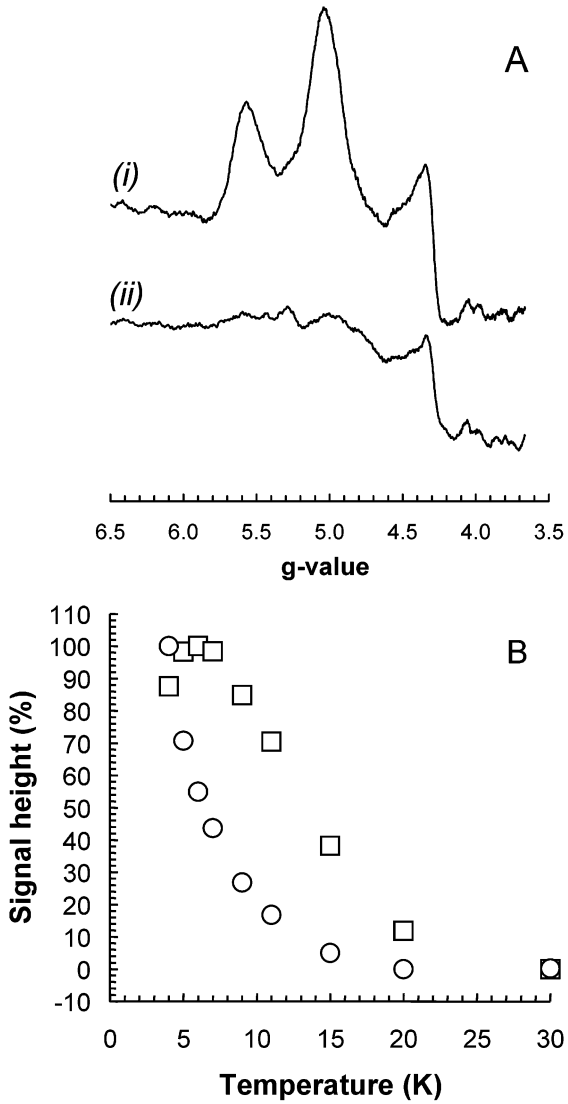


FIGURE 2: (A) EPR spectra of dithionite-reduced purified NarGHI (i) and apomolybdo-NarGHI (ii) around $g = 5.0$. Spectra were recorded under the following EPR conditions: temperature, 9 K; microwave power, 100 mW at 9.381 GHz; modulation amplitude, 10 $G_{pp}$ at 100 kHz. Spectra are corrected for the variation in protein concentration between the two samples. (B) Temperature dependence of the $g = 5.023$ (squares) and $g = 5.556$ (circles) features of the NarGHI EPR spectrum. EPR spectra were recorded as described for (A), except that the microwave power used was 20 mW. Signal intensities were normalized to a 0−100% scale.

Figure 2A (i) shows an EPR spectrum recorded at 9.0 K of dithionite-reduced purified NarGHI around $g = 5.0$. Noticeable in this spectrum are peaks at $g = 5.023$ and $g = 5.556$. These spectral features are almost completely eliminated in the spectrum of purified apomolybdo-NarGHI [Figure 2A (ii)]. A small peak-trough attributable to adventitiously bound high-spin $Fe^{3+}$ is observed in both spectra at around $g = 4.3$. Figure 2B shows that the $g = 5.023$ and $g = 5.556$ features exhibit distinct temperature dependences, with the former feature having a temperature optimum at approximately 6 K, whereas that of the latter is less than 4 K. The low-field features of the EPR spectrum are similar to those of a range of proteins containing a $[4Fe\text{-}4S]^{+}$ cluster with an $S = {}^{3}/_{2}$ ground state (*35*, *37*, *38*) and are consistent with NarGHI containing such a cluster (see Discussion).

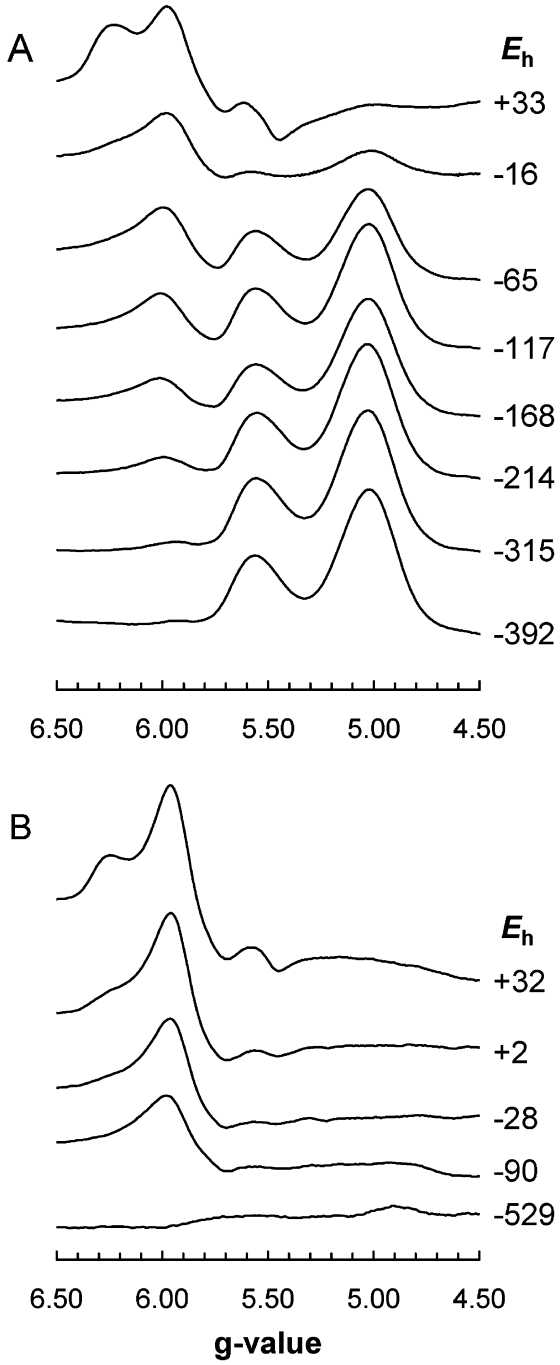


FIGURE 3: EPR spectra of samples from redox-poised membranes enriched in NarGHI (A) and apomolybdo-NarGHI (B). Samples were prepared as described in the Materials and Methods in 100 mM Tricine and 5 mM EDTA (pH 8.0). The redox potentials at which the samples were poised are indicated to the right of each spectrum. Membranes enriched in NarGHI were obtained from LCB79/pVA700 cells, whereas those enriched in apomolybdo-NarGHI were obtained from TP1000/pVA700. EPR conditions were as described for Figure 2A. Spectra were normalized to a nominal protein concentration of approximately 30 mg $mL^{-1}$.

*Potentiometric Analysis of the Low-Field NarGHI Spectrum*. To determine the midpoint potential of the $g = 5.023$ and $g = 5.556$ features of the EPR spectrum of reduced NarGHI, we performed redox titrations on enriched membrane fractions containing the native and apomolybdo forms of the enzyme. Figure 3 shows EPR spectra of redox-poised samples enriched in NarGHI (Figure 3A) and apomolybdo-

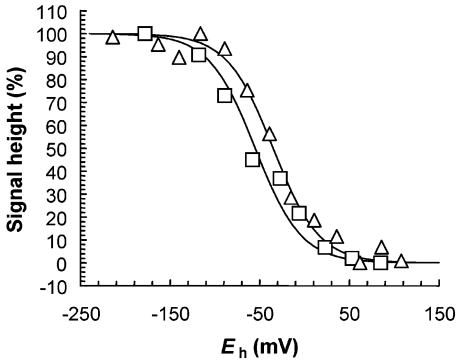


FIGURE 4: Determination of the midpoint potential of the low-field EPR features in wild-type (squares) and NarH-C16A mutant (triangles) NarGHI. Peak heights ($g = 5.023$) were determined by a three-point drop line method from spectra such as those presented in Figure 3A. Data were fitted to a single $n = 1.0$ species with $E_m$ values of −55 mV (wild type) and −35 mV (NarH-C16A mutant) at pH 8.0.

NarGHI (Figure 3B). Inspection of the spectra of Figure 3A indicates that the $g = 5.023$ and $g = 5.556$ features of the NarGHI spectrum are completely absent in oxidized samples and appear between approximately −16 and −117 mV. As is the case for the purified apomolybdo-NarGHI [Figure 2A (ii)], spectra of membranes enriched in this form of the enzyme do not exhibit significant features in the $g = 5.0-5.6$ region. For membranes enriched in either enzyme, features attributable to high-spin heme are visible around $g = 6.0$ at high potentials. These presumably arise from high-potential ligand binding cytochromes in the membrane samples such as cytochrome *bd* (*39*) and $bo_3$ (*40*). The $g = 5.023$ peak titrates with an $E_m$ of −55 mV at pH 8.0 (Figure 4).

The effect of the absence of the Mo-bisMGD cofactor on the low-field NarGHI EPR spectrum is consistent with the $g = 5.023$ and $g = 5.556$ peaks arising from a reduced cluster whose presence is cofactor-dependent or whose environment is significantly altered in the apomolybdoenzyme. It is known that the absence of cofactor in the apomolybdoenzyme causes a significant shift in the $E_m$ of FS1, eliciting a $\Delta E_m$ of approximately −50 mV (*7*). Using a similar strategy, we therefore investigated the effect on the line shape and redox potentiometry of the low-field signals of a mutant of NarH (NarH-C16A) in which FS1 is not detectable by EPR (*13*). The EPR spectrum in the low-field region of the dithionite-reduced NarH-C16A mutant is identical to that of the wild type (data not shown). However, a modest $\Delta E_m$ of +20 mV is elicited by the mutation (Figure 4), suggesting that absence of EPR-detectable FS1 may have a subtle effect on the redox chemistry of FS0.

*EPR Analysis of the NarH [4Fe-4S] Clusters*. Previous potentiometric analyses of the NarGHI [Fe-S] clusters indicated that they have $E_m$ values of +130 mV (FS1), −420 mV (FS2), −55 mV (FS3), and +180 mV (FS4) at pH 8.0 (*7*). The species giving rise to the $g = 5.023$ and $g = 5.556$ features of the NarGHI spectrum coincidentally has an $E_m$ value of −55 mV. It is therefore important to eliminate the possibility that the new spectral features arise from a subpopulation of FS3 ($E_m = -55$ mV). It has also been speculated that a subpopulation of the spectral features assigned to FS1 may, in fact, arise from FS0 (see below) (*23*). This would be consistent with the $\Delta E_m$ elicited on FS1

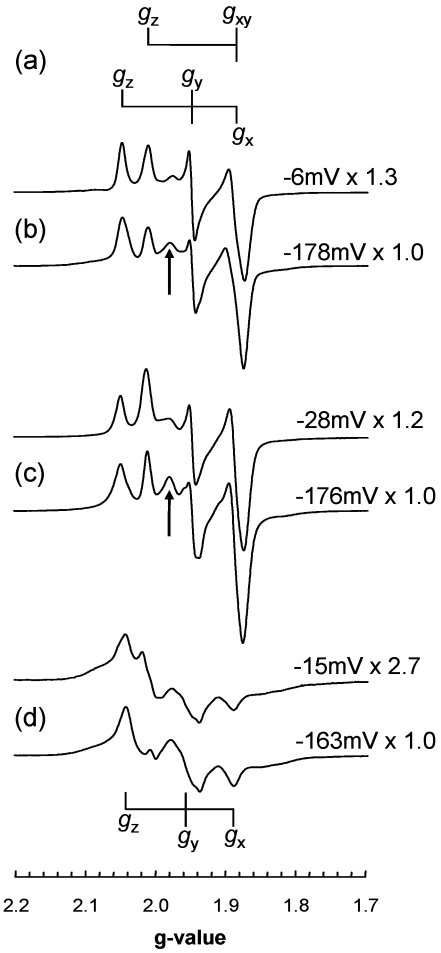


FIGURE 5: EPR spectra around $g = 2$ of redox-poised NarGHI, apomolybdo-NarGHI, and NarH-C16A mutant NarGHI in enriched membrane preparations. (a) Because of its magnetic isolation, Guigliarelli et al. (*15*) were able to simulate the spectrum of FS1 as the sum of two components, a major rhombic component with $g_z = 2.05$, $g_y = 1.95$, $g_x = 1.88$ and a minor axial component with $g_z = 2.01$, $g_{xy} = 1.88$. (b) EPR spectra of redox-poised wild-type NarGHI. Potentials were chosen to illustrate spectra of samples in which FS1 is reduced and in magnetic isolation in the protein (−6 mV) and in which both FS1 and FS3 are reduced (−178 mV). (c) Similar spectra of redox-poised samples containing apomolybdo-NarGHI at $E_h = -28$ mV and $E_h = -176$ mV. For (b) and (c), the obvious contribution of FS3 to the low-potential spectrum is indicated by a vertical arrow. (d) Spectra of redox-poised NarH-C16A mutant NarGHI which lacks EPR-detectable FS1. FS3 exhibits a rhombic EPR spectrum with $g_z = 2.04$, $g_y = 1.96$, $g_z = 1.88$. EPR spectra were recorded at 12 K and 20 mW for (b) and (c) and 100 mW for (d). Other EPR conditions were as described for Figure 1.

by the absence of Mo-bisMGD (*7*). To address these issues, we reexamined the EPR properties in the $g = 2$ region of wild-type, apomolybdo, and NarH-C16A mutant NarGHI.

Figure 5a illustrates the $g$ values of the two $S = {}^1/_2$ species attributed to FS1 by Guigliarelli et al. (*15*). Figure 5b shows EPR spectra of redox-poised wild-type NarGHI at a potential where the spectrum of FS1 predominates ($E_h = -6$ mV) and at one where FS3 also contributes ($E_h = -178$ mV). It is clear from inspection of the higher potential spectrum that FS1 in membrane samples exhibits spectral features essentially identical to those reported by Guigliarelli et al. (*15*) (cf. Figure 5a and 5b). The absence of cofactor in apomolybdo-NarGHI has only subtle effects on the EPR line shape of reduced FS1 (at $E_h = -28$ mV) and the super-

position of reduced FS1 *plus* FS3 in more reduced samples ($E_h = -176$ mV) (Figure 5c).

Major differences are elicited by the NarH-C16A mutation on the EPR properties of partially reduced NarGHI. This mutation results in the absence of EPR-detectable FS1 in NarGHI (*13*), rendering FS3 the highest potential [4Fe-4S] cluster with EPR features around $g = 2.0$. Figure 5d illustrates spectra of FS3 at two $E_h$ values in the absence of FS1. It is clear that the two components illustrated in Figure 5a are completely absent in a NarH-C16A mutant, consistent with both subpopulations of the highest potential [4Fe-4S] cluster of NarGHI arising from FS1 (*15*), rather than with one of them arising from FS0 (*23*).

The features of the spectrum of FS3 are consistent with them arising from a rhombic species with $g_z = 2.04$, $g_y = 1.96$, and $g_z = 1.88$ (Figure 5d). However, the spectrum exhibits broad "wings" which comprise a broad peak at approximately $g = 2.09$ and a broad trough at $g = 1.83$. These observations suggest that FS3 is not magnetically isolated at the potentials used to generate the spectra of Figure 5d ($E_h = -15$ and $-163$ mV). Similar broad wings are observed in reduced seven-iron ferredoxins in which a spin−spin interaction occurs between the $S = {}^1/_2$ [4Fe-4S] cluster under scrutiny and an $S = 2$ [3Fe-4S] cluster with which it is spin-coupled (*41*, *42*). It is noteworthy that FS3 forms half of a 7Fe ferredoxin-like pair (with FS4, the [3Fe-4S] cluster) in the structure of NarGHI (*2*).

To compare the potentiometric behavior of the high-spin signals with those of the reduced $S = {}^1/_2$ [4Fe-4S] clusters, we performed potentiometric analyses of the NarGHI EPR spectrum around $g = 2.0$ at 12 K. Figure 6 shows potentiometric titrations of the highest potential [4Fe-4S] clusters (FS1 and FS3) in NarGHI, apomolybdo-NarGHI, and the NarH-C16A mutant. As has previously been reported by us (*7*), loss of Mo-bisMGD results in a 50 mV decrease in the potential of FS1 from +130 to +80 mV. FS3 is the highest potential [4Fe-4S] cluster in the NarH-C16A mutant, and it titrates with an $E_m$ of $-50$ mV, in reasonable agreement with its reported potential in the wild-type enzyme (*7*). This potential is sufficiently resolved from that of the low-field features in this mutant for us to conclude that the low-field species arises from a different cluster. In all forms of NarGHI studied herein, the reduction of FS2 (the $E_m = -420$ mV [4Fe-4S] cluster) is manifested by a significant broadening of the overall EPR spectrum as a result of strong spin−spin interactions between the multiple paramagnetic clusters present. Its potential can therefore be estimated from the attenuation of features assigned to FS1 and/or FS3 as FS2 becomes reduced. In NarGHI, apomolybdo-NarGHI, and the NarH-C16A mutant, we estimate the $E_m$ of FS2 to be approximately $-420$ to $-430$ mV (data not shown; Table 2).

To complete the potentiometric picture of the FS3 to Mo-bisMGD segment of the NarGHI electron transfer pathway, we also determined the $E_m$ values of the Mo(IV/V) and Mo(V/VI) couples at 150 K in the forms of the enzyme used herein. The apomolybdoenzyme does not exhibit any EPR-detectable Mo(V), and the NarH-C16A mutant has little or no effect on the molybdenum potentials [the estimated $E_m$ for the Mo(IV/V) and Mo(V/VI) are approximately 100 and 200 mV, respectively, based on the potentiometric behavior of the $g = 1.98$ peak of the "high-pH" form of the Mo(V) spectrum]. Finally, for each enzyme studied, the $E_m$ of the [3Fe-4S] cluster was determined by analysis of the potentiometric behavior of its $g = 2.02$ peak at 12 K. In each case, its $E_m$ was estimated to be approximately +180 to +185 mV. All of the potentiometric results generated herein are summarized in Table 2.

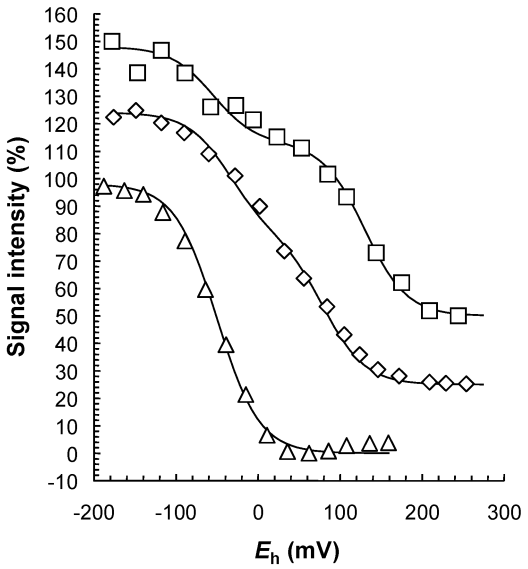


FIGURE 6: Potentiometric titrations of the highest potential NarGHI [4Fe-4S] clusters with spectral features around $g = 2.0$. Squares: titration of the $g_{xy}/g_x$ peak-trough ($g = 1.88$) of the spectrum of NarGHI. Data were fitted to two $n = 1.0$ species with $E_m$ values of +130 mV (63%; FS1) and $-55$ mV (35%; FS3). Diamonds: titration of the $g_{xy}/g_x$ peak-trough ($g = 1.88$) of the spectrum of apomolybdo-NarGHI. Data were fitted to two $n = 1.0$ species with $E_m$ values of +80 mV (55%; FS1) and $-35$ mV (44%; FS3). Triangles: titration of the $g_z$ peak *minus* the $g_x$ trough of the spectrum of NarH-C16A NarGHI. Data were fitted to a single $n = 1.0$ with species with an $E_m$ of $-50$ mV (FS3). EPR spectra were recorded as described for Figure 5, using 20 mW microwave power for the NarGHI and apomolybdo-NarGHI and 10 mW for NarH-C16A mutant NarGHI.

Table 2: Summary of [Fe-S] and Mo Potentiometric Data

| | center/couple $E_m$ (mV), pH 8.0 | | | | | | |
|---|---|---|---|---|---|---|---|
| enzyme | Mo(V/VI) | Mo(IV/V) | FS0 | FS1 | FS2 | FS3 | FS4 |
| NarGHI | 205[a] | 100 | −55 | +130 | −420 | −55 | +180 |
| apomolybdo-NarGHI | nd[b] | nd | nd | +80 | −430 | −35 | +185 |
| NarH-C16A NarGHI | 200 | 110 | −35 | nd | −420 | −50 | +185 |

[a] We estimate the experimental error in our estimates of $E_m$ values to be ±10 mV. Data are representative of at least two data sets. [b] Not detected.

*Structural Characterization of Apomolybdo-NarGHI*. To further rationalize the EPR results described herein, we determined the crystal structure of apomolybdo-NarGHI at 2.2 Å resolution. Its overall structure is highly similar to the native structure with a root mean square deviation (rmsd) of 0.29 Å for the superposition of 1240 NarG C-α atoms between the two forms [as determined with Swiss PDB-Viewer (*43*)]. The major structural changes are localized to the active site. As expected from spectroscopic and biochemical analyses (*7*), apomolybdo-NarGHI does not contain Mo-bisMGD. However, the electron density does reveal the presence of a guanosine diphosphate (GDP) in the same position as the guanine nucleotide moiety of the MGD-Q

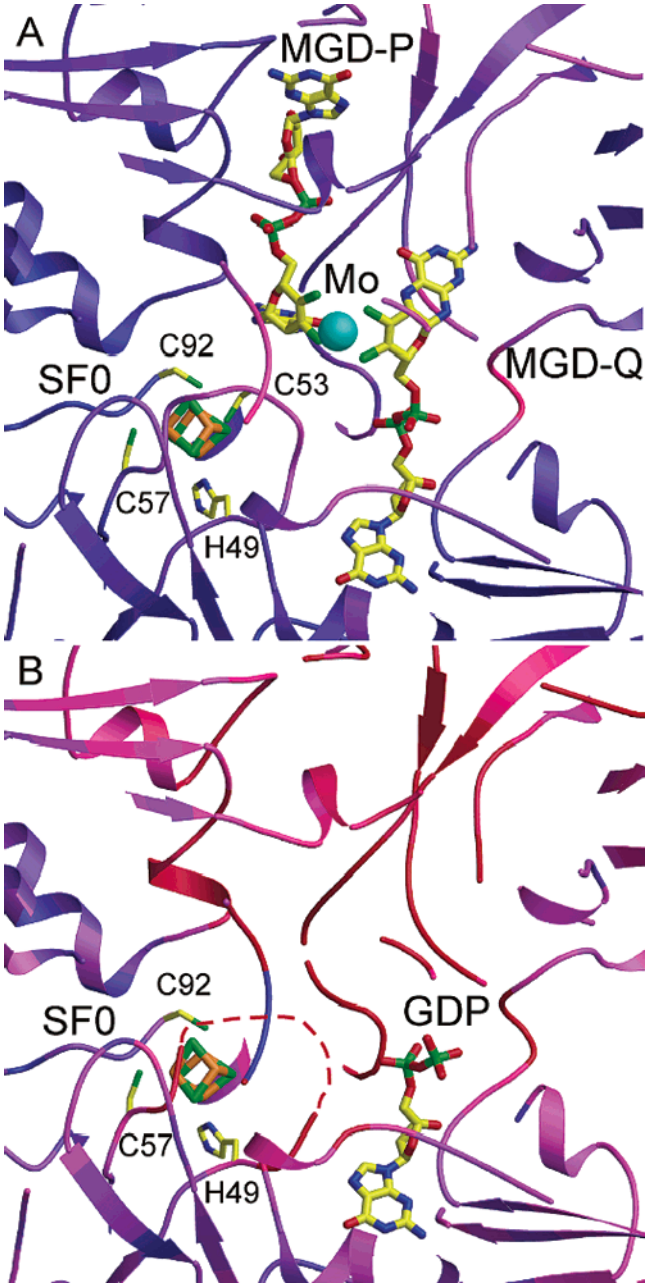


FIGURE 7: Detailed view of the cluster FS0 in the native NarGHI (A) and in the apomolybdo-NarGHI (B). Ribbon diagrams of the NarG structure surrounding FS0. Mo-bisMGD, FS0, and GDP are shown in stick rendering. Coloring reflects the temperature factor with a color ramp from blue to red indicating 10−40 Å$^2$ change. Electron density was not observed for residues 51−55 in the apomolybdo-NarGHI structure, and this sequence is represented as a dashed line in (B). The figure was prepared with Molscript (*54*) and rendered in Raster3D (*55*).

pterin in the native complex (cf. Figure 7A and 7B). Many of the residues that interact with the Mo-bisMGD in the native enzyme (NarG-D222, NarG-R260, NarG-S719, NarG-H1092, NarG-H1098, NarG-R1218) have side chains with large thermal parameters in the apomolybdo-NarGHI structure, suggesting high levels of motion in the absence of the cofactor (Figure 7B). Despite the absence of the high-spin EPR signal in the apomolybdo-NarGHI, the electron density map clearly reveals the presence and relative structural integrity of the FS0 cluster. Three of the FS0-coordinating residues are clearly visible, NarG-H49, NarG-C57, and NarG-C92, which superpose very well with the corresponding three residues in the native NarG. However, in apomolybdo-NarGHI, a major structural difference is the greater conformational freedom of a sequence of NarG residues (51−55) which contains the FS0 ligand NarG-C53 (Figure 7B). This loop is well ordered in the native structure and lies in close proximity to the Mo-bisMGD cofactor (Figure 7A). In addition, the FS0 cluster refines with a lower occupancy (0.5, with an overall temperature factor of 27.8 Å$^2$), indicating that the cluster is less tightly coordinated to the apomolybdo enzyme than to native NarGHI (refined to an occupancy of 1.0 with an overall temperature factor of 21.5 Å$^2$).

## DISCUSSION

NarGHI exhibits a range of EPR spectra observable at liquid helium temperatures (4−20 K), ranging from fairly typical [Fe-S] cluster spectra located in the $g = 2.0$ region (*6*, *7*, *14*, *15*) to HALS ferric heme spectra in the $g = 3.0$−4.0 range. At higher temperatures (>50 K), the molybdenum of the Mo-bisMGD is also readily observable in its Mo(V) state (*4*, *44*). Although the NarG subunit of NarGHI contains a Cys group located toward its N-terminus, there has been a conspicuous absence of obvious EPR evidence for the presence of a [4Fe-4S] cluster in this subunit.

Low-field EPR features in spectra of [4Fe-4S] clusters have been reported for a range of proteins/enzymes, including *Pyrococcus furiosus* ferredoxin (fer_pyrfu) (*35*, *45*, *46*), the iron protein of the *Azotobacter vinelandii* nitrogenase iron protein (nih1_azovi) (*38*), in the eight-iron form of *Desulfovibrio africanus* ferredoxin III (fer3_desaf) (*47*), and a FrdB-C151S mutant of the electron transfer subunit (frdb_ecoli) of *E. coli* fumarate reductase (FrdABCD) (*37*). Spectra of all of these proteins in their reduced states typically exhibit two peaks with $g$ values similar to those of the two peaks in the low-field EPR spectra of NarGHI reported herein, and these features are typically assigned to a [4Fe-4S] cluster with an $S = {}^3/_2$ ground state. Theoretical considerations of the origin of the two peaks are based on the work of Hagen (*36*), which resulted in the generation of rhombograms depicting possible $g$ values for each of the three $g$ tensors for $\Delta S = \pm{}^1/_2$ and $\Delta S = \pm{}^3/_2$ transitions as a function of the rhombicity ($E/D$, where $E$ and $D$ are the rhombic and axial zero-field splitting parameters, respectively) of the system under scrutiny. Analysis of the rhombograms presented by Hagen (*36*) suggests that the $g = 5.023$ peak arises from a $\Delta S = \pm{}^1/_2$ transition, whereas the $g = 5.556$ peak arises from a $\Delta S = \pm{}^3/_2$ transition. For an $E/D$ value of approximately 0.22−0.24, the predicted values for the low-field $g$ tensors of the $\Delta S = \pm{}^1/_2$ and $\Delta S = \pm{}^3/_2$ closely approximate those observed for the NarGHI $g = 5.023$ and $g = 5.556$ peaks. This assignment is also consistent with the temperature dependences of the two spectral features: the $g = 5.556$ peak has an optimum temperature for detection below that attainable by the cryostat of the EPR instrumentation used herein.

The $E_m$ value of the high-spin [4Fe-4S] cluster spectrum is approximately −55 mV, which is coincidentally the same as that of the FS3 cluster located in NarH. However, the fact that the new spectral features are essentially eliminated in apomolybdo-NarGHI strongly argues in favor of them arising from a cluster that is located in close juxtaposition

to the Mo-bisMGD cofactor. However, previous work has suggested that FS1 is also affected by the absence of the cofactor (*7*). In the first thorough potentiometric characterization of NarGHI by EPR, it was found that the spectral features assigned to FS1 appear to arise from two independent subpopulations with identical $E_m$ values (*15*). On the basis of studies of dimethyl sulfide dehydrogenase from *Rhodovulum sulfidophilum*, an enzyme with a very similar catalytic subunit to that of NarGHI, it has been suggested that one of the FS1 subpopulations may arise from FS0 (*23*). We addressed this question by (i) confirming the presence of the new high-spin signals in a NarH-C16A mutant, (ii) confirming the absence in the NarH-C16A mutant of all the spectral features assigned to FS1 by Guigliarelli et al. (*15*), and (iii) demonstrating a separation of the low-field and FS3 $E_m$ values in a NarH-C16A mutant. On the basis of these observations, we assign the $g = 5.023$ and $g = 5.556$ peaks to the FS0 [4Fe-4S] cluster of NarG.

To corroborate our assignment of the high-spin features of the NarGHI EPR spectrum to FS0, we determined the crystal structure of the apomolybdoenzyme at 2.2 Å resolution (Figure 7). FS0 is still present in this structure (Figure 7B), albeit in a form less tightly coordinated by the surrounding protein environment. Two obvious explanations exist for our inability to observe the EPR spectrum of FS0 in this form of the enzyme. (i) Solvent exposure of FS0 via the Mo-bisMGD binding pocket may lower the $E_m$ of FS0 to the extent that it is not reducible at readily accessible $E_h$ values, which are limited to approximately −530 mV at pH 8. (ii) The increased thermal disorder in the structure implied by the absence of electron density for residues 51−55 of NarG could lead to significant structural heterogeneity in the environment of FS0, resulting in its spectrum being broadened to the extent that it is rendered EPR invisible. This is also likely to result in heterogeneous redox chemistry, making the $E_m$ of FS0 in apomolybdo-NarGHI poorly defined.

The factors that result in a [4Fe-4S] cluster having a high-spin ground state are currently poorly understood. Such clusters are almost always associated with non-cysteinyl coordination. Typical high-spin clusters have coordination provided by three Cys residues and one alternative amino acid such as Asp or Ser (*35*, *37*). A good example of such coordination is provided by *P. furiosus* ferredoxin (*35*, *45*). The reduced wild-type form of this protein contains a single $[4Fe\text{-}4S]^+$ cluster which has two populations of ground states, one with $S = {}^1/_2$ and the other with $S = {}^3/_2$ (*45*). The EPR spectrum of the high-spin form of this cluster is essentially identical to that observed for FS0: it has peaks at approximately $g = 5.0$ and 5.6. In a D14C mutant (of the second cluster coordinating residue), the cluster becomes homogeneously low spin (*46*). In *E. coli* fumarate reductase (FrdABCD), a [4Fe-4S] cluster is coordinated by four Cys residues in the electron transfer subunit (FrdB) (*48*). Mutation of the second of these to a Ser results in a change in spin state from low to high spin (*37*). The His residue coordinating FS0 in NarG has also been subjected to site-directed mutagenesis to Cys and Ser (*4*). Although the [Fe-S] clusters of NarGHI were investigated by EPR in a NarG-H49C mutant, no obvious evidence for new spectral features arising from an $S = {}^1/_2$ form of FS0 was found, suggesting that the change in coordination does not change its spin state.

We have previously demonstrated that the absence of Mo-bisMGD in apomolybdo-NarGHI perturbs the redox chemistry of FS1 (*7*), causing a 50 mV decrease in its $E_m$. We extended these studies herein by examining the effect of the lack of EPR-detectable FS1 (in a NarH-C16A mutant) on the redox chemistry of both FS0 and the Mo(IV/V/VI) couples of the Mo-bisMGD cofactor. A minor effect was elicited on the $E_m$ of FS0, but no effect was observed on the Mo-bisMGD cofactor. These results can be explained by the rather large structural differences expected between NarGHI and apomolybdo-NarGHI in the region of the Mo-bisMGD binding site. The edge-to-edge distance between FS1 and the MGD-P pterin is approximately 12.2 Å, whereas that between FS1 and FS0 is 11.2 Å. Thus, it is possible that the effect of the absence of cofactor could be propagated to both clusters. In the former case a mild perturbation results in the observed drop in its $E_m$, whereas in the latter, a large perturbation results in the nonobservance of its EPR spectrum.

As revealed by the presence of a GDP moiety in the MGD-Q binding site, it is clear that at least the guanine nucleotide can be assembled into NarG in the absence of mature Mo-bisMGD. This phenomenon has also been detected biochemically in *Rhodobacter sphaeroides* $Me_2SO$ reductase (*49*), in which two nucleotides are detected in the apomolybdoenzyme. It is also notable that the overall structure of NarG in apomolybdo-NarGHI is essentially identical to that found in the native enzyme. This observation has implications for the role of the fourth open reading frame within the *nar* operon (*narJ*). NarJ is a system-specific chaperone that is synthesized in substoichiometric amounts compared to the subunits of the mature enzyme (*50*, *51*). It is hypothesized to hold NarG in a cofactor binding competent conformation during enzyme maturation. It is clear from the structural data presented herein that NarJ does not remain associated with membrane-bound apomolybdo-NarGHI and that enzyme that bypasses the Mo-bisMGD insertion step of the maturation process adopts a structure that is essentially identical to that of the native enzyme.

Overall, we have observed the EPR spectrum of FS0 in NarGHI and have demonstrated that this spectrum arises from a [4Fe-4S] cluster with an $S = {}^3/_2$ ground state. The observation and potentiometric characterization of this cluster complete the initial characterization of the entire electron transfer chain through NarGHI from the quinol binding sites of NarI (*3*, *10*, *52*) to the Mo-bisMGD cofactor of NarG. These studies represent an important step in understanding the electron transfer pathway connecting the [Fe-S] clusters of NarH and the Mo-bisMGD cofactor of NarG.

## ACKNOWLEDGMENT

The authors thank Delilah Mroczko for operating the B. Braun Biostat B fermentation system. M.B. and N.S. thank the Department of Energy and the Howard Hughes Medical Institute for access to beamline 8.2.1 at the Advanced Light Source, Berkeley, CA.

## REFERENCES

1. Blasco, F., Guigliarelli, B., Magalon, A., Asso, M., Giordano, G., and Rothery, R. A. (2001) The coordination and function of the redox centres of the membrane-bound nitrate reductases, *Cell. Mol. Life Sci. 58*, 179−193.

2. Bertero, M. G., Rothery, R. A., Palak, M., Hou, C., Lim, D., Blasco, F., Weiner, J. H., and Strynadka, N. C. (2003) Insights into the respiratory electron transfer pathway from the structure of nitrate reductase A, *Nat. Struct. Biol. 10*, 681−687.
3. Rothery, R. A., Blasco, F., Magalon, A., Asso, M., and Weiner, J. H. (1999) The hemes of *Escherichia coli* nitrate reductase A (NarGHI): potentiometric effects of inhibitor binding to NarI, *Biochemistry 38*, 12747−12757.
4. Magalon, A., Asso, M., Guigliarelli, B., Rothery, R. A., Bertrand, P., Giordano, G., and Blasco, F. (1998) Molybdenum cofactor properties and [Fe-S] cluster coordination in *Escherichia coli* nitrate reductase A: investigation by site-directed mutagenesis of the conserved His-50 residue in the NarG subunit, *Biochemistry 37*, 7363−7370.
5. Magalon, A., Lemesle-Meunier, D., Rothery, R. A., Frixon, C., Weiner, J. H., and Blasco, F. (1997) Heme axial ligation by the highly conserved His residues in helix II of cytochrome $b_{nr}$ of *Escherichia coli* nitrate reductase A (NarGHI), *J. Biol. Chem. 272*, 25652−25658.
6. Guigliarelli, B., Magalon, A., Asso, M., Bertrand, P., Frixon, C., Giordano, G., and Blasco, F. (1996) Complete coordination of the four Fe-S centres of the $\beta$ subunit from *Escherichia coli* nitrate reductase. Physiological, biochemical and EPR characterization of site-directed mutants lacking the highest or lowest potential [4Fe-4S] clusters, *Biochemistry 35*, 4828−4836.
7. Rothery, R. A., Magalon, A., Giordano, G., Guigliarelli, B., Blasco, F., and Weiner, J. H. (1998) The molybdenum cofactor of *Escherichia coli* nitrate reductase A (NarGHI): effect of a *mobAB* mutation and interactions with [Fe-S] clusters, *J. Biol. Chem. 273*, 7462−7469.
8. Rothery, R. A., Blasco, F., and Weiner, J. H. (2001) Electron transfer from heme $b_L$ to the [3Fe-4S] cluster of *Escherichia coli* nitrate reductase A (NarGHI), *Biochemistry 40*, 5260−5268.
9. Giordani, R., Buc, J., Cornish-Bowden, A., and Cárdenas, M. L. (1997) Kinetics of membrane-bound nitrate reductase A from *Escherichia coli* with analogs of physiological electron donors. Different reaction sites for menadiol and duroquinol, *Eur. J. Biochem. 250*, 567−577.
10. Zhao, Z., Rothery, R. A., and Weiner, J. H. (2003) Transient Kinetic Studies of Heme Reduction in *Escherichia coli* Nitrate Reductase A (NarGHI) by Menaquinol, *Biochemistry 42*, 5403−5413.
11. Jormakka, M., Tornroth, S., Byrne, B., and Iwata, S. (2002) Molecular basis of proton motive force generation: structure of formate dehydrogenase-N, *Science 295*, 1863−1868.
12. Augier, V., Guigliarelli, B., Asso, M., Bertrand, P., Frixon, C., Giordano, G., Chippaux, M., and Blasco, F. (1993) Site-directed mutagenesis of conserved cysteine residues within the $\beta$ subunit of *Escherichia coli* nitrate reductase. Physiological, biochemical, and EPR characterization of the mutated enzymes, *Biochemistry 32*, 2013−2023.
13. Augier, V., Asso, M., Guigliarelli, B., More, C., Bertrand, P., Santini, C., Blasco, F., Chippaux, M., and Giordano, G. (1993) Removal of the high-potential [4Fe-4S] center of the $\beta$-subunit from *Escherichia coli* nitrate reductase. Physiological, biochemical, and EPR characterization of site-directed mutated enzymes, *Biochemistry 32*, 5099−5108.
14. Johnson, M. K., Bennett, D. E., Morningstar, J. E., Adams, M. W. W., and Mortenson, L. E. (1985) The iron−sulfur cluster composition of *Escherichia coli* nitrate reductase, *J. Biol. Chem. 260*, 5456−5463.
15. Guigliarelli, B., Asso, M., More, C., Augier, V., Blasco, F., Pommier, J., Giordano, G., and Bertrand, P. (1992) EPR and redox characterization of the iron−sulfur centres in nitrate reductases A and Z from *Escherichia coli*. Evidence of a high and low potential class and their relevance in the electron-transfer mechanism, *Eur. J. Biochem. 207*, 61−68.
16. Breton, J., Berks, B. C., Reilly, A., Thomson, A. J., Ferguson, S. J., and Richardson, D. J. (1994) Characterization of the paramagnetic iron-sontaining redox centres of *Thiosphaera pantotropha* periplasmic nitrate reductase, *FEBS Lett. 345*, 76−80.
17. Dias, J. M., Than, M. E., Humm, A., Huber, R., Bourenkov, G. P., Bartunik, H. D., Bursakov, S., Calvete, J., Caldeira, J., Carneiro, C., Moura, J. J., Moura, I., and Romao, M. J. (1999) Crystal structure of the first dissimilatory nitrate reductase at 1.9 Å solved by MAD methods, *Struct. Folding Des. 7*, 65−79.
18. Boyington, J. C., Gladyshev, V. N., Khangulov, S. V., Stadtman, T. C., and Sun, P. D. (1997) Crystal structure of formate dehydrogenase H: catalysis involving Mo, molybdopterin, selenocyteine, and an [4Fe-4S] cluster, *Science 275*, 1305−1308.
19. Gladyshev, V. N., Boyington, J. C., Khangulov, S. V., Grahame, D. A., Stadtman, T. C., and Sun, P. C. (1996) Characterization of crystalline formate dehydrogenase H from *Escherichia coli*. Stabilization, EPR spectroscopy, and preliminary crystollographic analysis, *J. Biol. Chem. 271*, 8095−8100.
20. Cammack, R., and Weiner, J. H. (1990) Electron paramagnetic resonance spectroscopic characterization of dimethyl sulfoxide reductase of *Escherichia coli*, *Biochemistry 29*, 8410−8416.
21. Rothery, R. A., and Weiner, J. H. (1996) Interaction of an engineered [3Fe-4S] cluster with a menaquinol binding site of *Escherichia coli* DMSO reductase, *Biochemistry 35*, 3247−3257.
22. Trieber, C. A., Rothery, R. A., and Weiner, J. H. (1996) Engineering a novel iron−sulfur cluster into the catalytic subunit of *Escherichia coli* dimethyl-sulfoxide reductase, *J. Biol. Chem. 271*, 4620−4626.
23. McDevitt, C. A., Hanson, G. R., Noble, C. J., Cheesman, M. R., and McEwan, A. G. (2002) Characterization of the redox centers in dimethyl sulfide dehydrogenase from *Rhodovulum sulfidophilum*, *Biochemistry 41*, 15234−15244.
24. Volbeda, A., Charon, M.-H., Piras, C., Hatchikian, E. C., Frey, M., and Fontecilla-Camps, J. C. (1995) Crystal structure of the nickel−iron hydrogenase from *Desulfovibrio gigas*, *Nature 273*, 580−587.
25. Peters, J. W., Lanzilotta, W. N., Lemon, B. J., and Seefeldt, L. C. (1998) X-ray crystal structure of the Fe-only hydrogenase (CpI) from *Clostridium pasteurianum* to 1.8 angstrom resolution, *Science 282*, 1853−1858.
26. Pascal, M. C., Burini, J. F., Ratouchniak, J., and Chippaux, M. (1982) Regulation of the nitrate reductase operon: effect of mutations in chlA, B, D and E genes, *Mol. Gen. Genet. 188*, 103−106.
27. Palmer, T., Santini, C., Iobbi-Nivol, C., Eaves, D. J., Boxer, D. H., and Giordano, G. (1996) Involvement of the *narJ* and *mob* gene products in distinct steps in the biosynthesis of the molybdoenzyme nitrate reductase in *Escherichia coli*, *Mol. Microbiol. 20*, 875−884.
28. Sambrook, J., Fritsch, E. F., and Maniatis, T. (1989) *Molecular Cloning: A Laboratory Manual*, 2nd ed., Cold Spring Harbor Laboratory Press, Cold Spring Harbor, NY.
29. Rothery, R. A., and Weiner, J. H. (1991) Alteration of the iron−sulfur composition of *Escherichia coli* dimethyl sulfoxide reductase by site-directed mutagenesis, *Biochemistry 30*, 8296−8305.
30. Lowry, O. H., Rosebrough, N. J., Farr, A. L., and Randall, R. J. (1951) Protein determination with the Folin reagent, *J. Biol. Chem. 191*, 265−275.
31. Markwell, M. A. D., Haas, S. M., Bieber, L. L., and Tolbert, N. E. (1978) A modification of the Lowry procedure to simplify protein determination in membrane and lipoprotein samples, *Anal. Biochem. 87*, 206−210.
32. Otwinowski, Z., and Minor, W. (1997) Processing of X-ray Diffraction Data Collected in Oscillation Mode, *Methods Enzymol. 276*, 307−326.
33. Brunger, A. T., Adams, P. D., Clore, G. M., DeLano, W. L., Gros, P., Grosse-Kunstleve, R. W., Jiang, J. S., Kuszewski, J., Nilges, M., Pannu, N. S., Read, R. J., Rice, L. M., Simonson, T., and Warren, G. L. (1998) Crystallography & NMR system: A new software suite for macromolecular structure determination, *Acta Crystallogr., Sect. D: Biol. Crystallogr. 54*, 905−921.
34. McRee, D. E. (1999) XtalView/Xfit−A versatile program for manipulating atomic coordinates and electron density, *J. Struct. Biol. 125*, 156−165.
35. Duderstadt, R. E., Brereton, P. S., Adams, M. W., and Johnson, M. K. (1999) A pure $S = {}^3/_2$ $[Fe_4S_4]^+$ cluster in the A33Y variant of *Pyrococcus furiosus* ferredoxin, *FEBS Lett. 454*, 21−26.
36. Hagen, W. R. (1992) EPR spectroscopy of iron−sulfur proteins, *Adv. Inorg. Chem. 38*, 165−222.
37. Kowal, A. T., Werth, M. T., Manadori, A., Cecchini, G., Schröder, I., Gunsalus, R. P., and Johnson, M. K. (1995) Effect of cysteine to serine mutations on the properties of the [4Fe-4S] center in *Escherichia coli* fumarate reductase, *Biochemistry 34*, 12284−12293.
38. Lindahl, P. A., Day, E. P., Kent, T. A., Orme-Johnson, W. H., and Munck, E. (1985) Mossbauer, EPR, and magnetization studies of the *Azotobacter vinelandii* Fe protein. Evidence for a $[4Fe\text{-}4S]^{1+}$ cluster with spin $S = {}^3/_2$, *J. Biol. Chem. 260*, 11160−11173.
39. Rothery, R. A., and Ingledew, W. J. (1989) The cytochromes of anaerobically grown *Escherichia coli*. An electron paramagnetic

resonance study of the cytochrome *bd* complex *in situ*, *Biochem. J. 261*, 437−443.
40. Salerno, J. C., Bolgiano, B., Poole, R. K., Gennis, R. B., and Ingledew, W. J. (1990) Heme-copper and heme-heme interactions in the cytochrome *bo*-containing quinol oxidase of *Escherichia coli*, *J. Biol. Chem. 265*, 4364−4368.
41. Armstrong, F. A., George, S. J., Thomson, A. J., and Yates, M. G. (1988) Direct electrochemistry in the characterisation of redox proteins: novel properties of *Azotobacter* 7Fe ferredoxin, *FEBS Lett. 234*, 107−110.
42. Hagen, W. R., Dunham, W. R., Johnson, M. K., and Fee, J. A. (1985) Quarter field resonance and integer-spin/half-spin interaction in the EPR of *Thermus thermophilus* ferredoxin. Possible new fingerprints for three iron clusters, *Biochim. Biophys. Acta 828*, 369−374.
43. Kaplan, W., and Littlejohn, T. G. (2001) Swiss-PDB Viewer (Deep View), *Brief. Bioinform. 2*, 195−197.
44. Vincent, S. P., and Bray, R. C. (1978) Electron paramagnetic resonance studies on nitrate reductase from *Escherichia coli* K12, *Biochem. J. 171*, 639−647.
45. Conover, R. C., Kowal, A. T., Fu, W. G., Park, J. B., Aono, S., Adams, M. W., and Johnson, M. K. (1990) Spectroscopic characterization of the novel iron−sulfur cluster in *Pyrococcus furiosus* ferredoxin, *J. Biol. Chem. 265*, 8533−8541.
46. Brereton, P. S., Duderstadt, R. E., Staples, C. R., Johnson, M. K., and Adams, M. W. (1999) Effect of serinate ligation at each of the iron sites of the [$Fe_4S_4$] cluster of *Pyrococcus furiosus* ferredoxin on the redox, spectroscopic, and biological properties, *Biochemistry 38*, 10594−10605.
47. George, S. J., Armstrong, F. A., Hatchikian, E. C., and Thomson, A. J. (1989) Electrochemical and spectroscopic characterization of the conversion of the 7Fe into the 8Fe form of ferredoxin III from *Desulfovibrio africanus*. Identification of a [4Fe-4S] cluster with one noncysteine ligand, *Biochem. J. 264*, 275−284.
48. Cammack, R., Patil, D. S., and Weiner, J. H. (1986) Evidence that centre 2 in *Escherichia coli* fumarate reductase is a [4Fe-4S] cluster, *Biochim. Biophys. Acta 870*, 545−551.
49. Temple, C. A., and Rajagopalan, K. V. (2000) Mechanism of assembly of the Bis(Molybdopterin guanine dinucleotide)molybdenum cofactor in *Rhodobacter sphaeroides* dimethyl sulfoxide reductase, *J. Biol. Chem. 275*, 40202−40210.
50. Blasco, F., Dos-Santos, J. P., Magalon, A., Frixon, C., Guigliarelli, B., Santini, C. L., and Giordano, G. (1998) NarJ is a specific chaperone required for molybdenum cofactor assembly in nitrate reductase A of *Escherichia coli*, *Mol. Microbiol. 28*, 435−447.
51. Liu, X., and DeMoss, J. A. (1997) Characterization of NarJ, a system-specific chaperone required for nitrate reductase biogenesis in *Escherichia coli*, *J. Biol. Chem. 272*, 24266−24271.
52. Rothery, R. A., Blasco, F., Magalon, A., and Weiner, J. H. (2001) The diheme cytochrome *b* subunit (NarI) of *Escherichia coli* nitrate reductase A (NarGHI): structure, function, and interaction with quinols, *J. Mol. Microbiol. Biotechnol. 3*, 273−283.
53. Thompson, J. D., Higgins, D. G., and Gibson, T. J. (1994) CLUSTAL W: improving the sensitivity of progressive multiple sequence alignment through sequence weighting, positions-specific gap penalties and weight matrix choice, *Nucleic Acids Res. 22*, 4673−4680.
54. Kraulis, P. J. (1991) MOLSCRIPT: A program to produce both detailed and schematic plots of protein structures, *J. Appl. Crystallogr. 24*, 946−950.
55. Merritt, E. A., and Bacon, D. J. (1997) Raster3D: Photorealistic molecular graphics, *Methods Enzymol. 277*, 505−524.

BI049938L